Near-exponential relationship between effective stress and permeability of porous rock revealed in Gangi's phenomenological models and application to gas shales

Ji-Quan Shi* and Sevket Durucan

Department of Earth Science and Engineering, Royal School of Mines, Imperial College London, London SW7 2BP, UK

*corresponding author: j.q.shi@imperial.ac.uk

Abstract

A number of theoretic models, as well as empirical equations obtained by fitting specific experimental data, have been developed to describe the relationship between effective stressand permeability of whole (intact) and fractured porous rock. It has been found that most experimental data can be fitted using exponential equations. In this study the modified power law equations by Gangi for intact and fractured rocks are revisited to evaluate their applicability for modeling experimental permeability data which display exponential or near-exponential effective stress dependency. It has been shown that Gangi's power law equations for both intact and fractured rock can be approximated, over the range of effective stresses of practical interest, by exponential equations with compressibilities that are related to the physical property of the rock. The significance of this work is that it has provided further theoretical evidence for the apparent exponential relationship between effective stress and permeability. Moreover, it allows for more vigorous theoretical equations to be applied with the easiness of empirical exponential equations. This is demonstrated by applying the models to the experimental permeability data for six gas shales reported recently.

Keywords: theoretical permeability models, empirical equations, exponential permeability equations, gas shale permeability

1. Introduction

Experimental studies on the variation of intact porous rock permeability with effective stress applied on the rock have been reported in the literature since 1950s (e.g. Fatt and Davies, 1952; Dobrynin, 1962; Gray et al., 1963; Knutson and Bohor, 1963; Kwon et al., 2001; Bustin et al. 2008; Dong et al., 2010; Heller et al., 2014). Empirical equations have been proposed to describe the experimental permeability data. They include exponential functions (e.g., Louis et al. 1977), power functions (e.g., Tiller, 1953; Kranz et al. 1979) and logarithmic functions (e.g. Dobrynin, 1962; Jones and Ovens, 1980).

As well as empirical equations, theoretical models have also been developed to describe the experimental data and predict the permeability behavior under stress. Gangi (1978) developed a phenomenological model, based upon the Hertzian theory of deformation of spheres, to predict the variation with effective stress with the permeability of whole (intact) porous rock. Gangi noted that if a porous rock is assume to be made up of a packing of spherical grains of uniform size, then its permeability will be a function of the square of the cross-sectional area

of its pores. Gangi further pointed out that permeability of the porous rock also depends upon the number of pore channels in a unit area perpendicular to the direction of flow and the number of pore channels per unit area is inversely proportional to the square of the sphere radius. Thus; if r_p is the pore radius and R is the spherical grain radius (see Figure 1a), the permeability of the porous rock in consideration will be given by

$$k \propto \frac{r_p^4}{R^2} \tag{1}$$

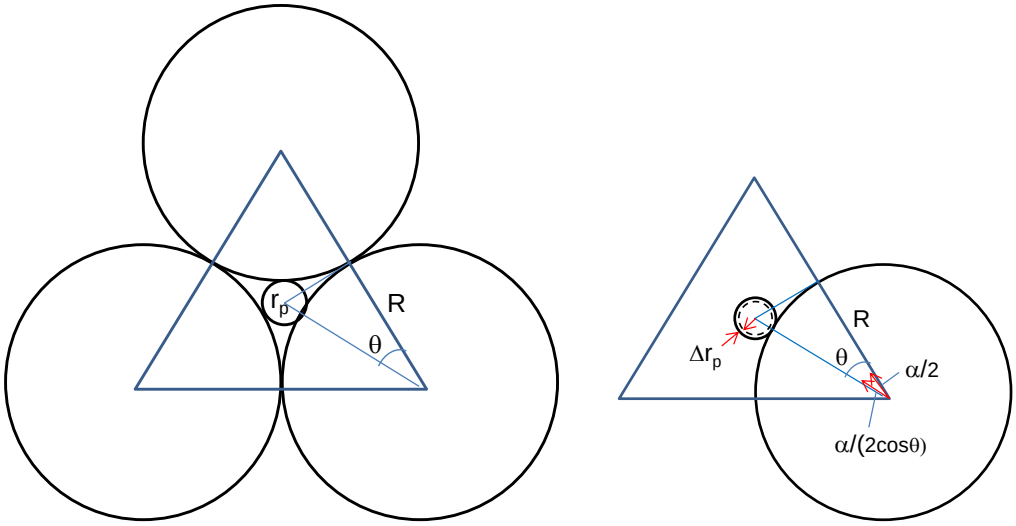

(a) (b)

Figure 1 a) A schematic of uniform grain packing for estimation of constant C_0; b) reduction in the pore radius caused by grain deformation (modified from Gangi, 1978).

Hertz theory gives change in separation, α, between sphere centres in a sphere packing due to an external force, F, as (Figure 2):

$$\frac{\alpha}{2R} = \left(\frac{a}{R}\right)^2 = \left[\frac{3(1-\upsilon^2)FR}{4E}\right]^{2/3}/R^2$$

$$= \left[\frac{3\pi(1-\upsilon^2)P}{4E}\right]^{2/3} = \left(\frac{P}{K_{gra}}\right)^{2/3} \tag{2}$$

where:

α = the "approach" (or change in separation) of the sphere centres;

R = the radius of the spherical grains;

d = the radius of the circle-of-contact of the spheres;

F = the external force;

E = the Young's modulus for the grains;

ν = the Poisson's ratio for the grains;

P = the external stress= $F/\pi R^2$;

K_{gra} = the effective elastic modulus for the grains given by

$$K_{gra} = \frac{4E}{3\pi(1-\upsilon^2)} = \frac{4K(1-2\upsilon)}{\pi(1-\upsilon^2)}$$

where K is the bulk modulus for the grains. Gangi noted that K_{gra} is typically of the same order of the grain material bulk modulus ($K_{gra} \approx 0.7K$ for $\nu \approx 0.25$).

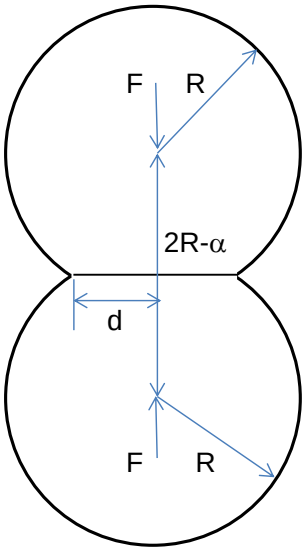

Figure 2 Sphere-sphere deformation considered in Hertz theory (after Gangi, 1978).

Gangi assumed, to a first approximation, that the pore shape does not change significantly (except in size) as P is increased and obtained the following expression for the reduction in the "pore radius" (Figure 1b)

$$\Delta r_p = c_1\alpha \cong 1/(2\cos\theta)\alpha. \tag{3}$$

Upon using Hertz's theory Equation (2), Equation (3) may be rearrange as

$$\Delta r_p = r_p\left(\frac{2c_1R}{r_p}\right)\left(\frac{\alpha}{2R}\right)$$

$$= r_pC_0\left(\frac{P}{K_{gra}}\right)^{2/3} \tag{4}$$

where $C_0 = 2c_1R/r_p$ is a constant depending upon the packing. Combining Equations (1) and (4), the following equation is obtained by Gangi

$$k_{wr} = k_{lp}[1 - C_0\left(\frac{P}{K_{gra}}\right)^{\frac{2}{3}}]^4 \tag{5}$$

where k_{lp} is the initial permeability of the loose-grain packing. Gangi recognised that in real rocks, there will be some cementation or permanent deformation of the grain contacts such that the radius (d in Figure 2) of the area-of-contact is not zero at zero stress. He pointed out

that this is equivalent to having some initial stress, P_i, acting on the rock and modified the equation accordingly,

$$k_{wr} = k_{lp}[1 - C_0\left(\frac{P+P_i}{K_{gra}}\right)^{\frac{2}{3}}]^4 \quad (6)$$

Although Equation (6) is derived based upon the assumption that the grains are all the same size spheres. Gangi argued that the same functional dependence would be expected even for a distribution of grain sizes. Gangi also pointed out that the underling Hertzian theory Equation (2) is unlikely to be valid for the effective stress P_e above $0.03K_{gra}$. However, given that K_{gra} is typically of the order of the grain bulk modulus, this would correspond, in general, to stresses as high as 10^5 psi (~69 MPa), well above the range of most measurements.

The response of fracture permeability in rocks to applied effective stress has also attracted a lot of interests from the research communities since 1970s (e.g. Jones, 1973; Nelson, 1975; Witherspoon and Gale, 1977). Both empirical equations and theoretical models have been developed to describe the experimental data and predict the fracture permeability behavior. It is commonly assumed in the derivation of the theoretical models that the fracture permeability is proportional to the cubic of its aperture.

Using a 'bed of nails' model (Figure 3a) for the asperities of a fracture, Gangi (1978) developed a model to describe the permeability variation of a fracture (or a fractured rock) with applied stress. In his derivation Gangi considered a simple power-law variation for the asperity-length distribution,

$$N(x) = I_0\left(\frac{x}{w_0}\right)^{n-1}, 1 < n < \infty \quad (7)$$

where $N(x)$ gives the number of rods whose shortness (the difference between its height l_i and the height of the largest rod w_0) is less than x, and I_0 is the total number of rod asperities. The exponent n cannot take on values less than one because the number of rods is finite when x = 0.

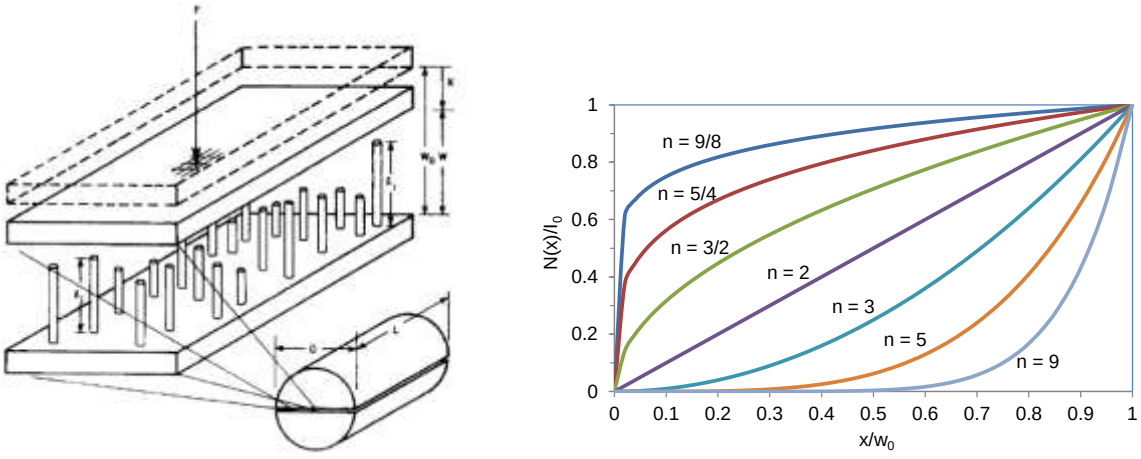

(a) (b)

Figure 3 a) A schematic of "bed of nail" model; b) Power-law asperity-shortness distribution functions (after Gangi, 1978).

These power-law distribution functions are plotted in Figure 3b. Gangi pointed out that while more complicated distribution functions might be needed and could be used, these distribution functions cover all the important characteristics that can be expected for fracture surfaces. For example, a very smooth surface with only a very few short asperities (or very few with large shortness) would be characterised by a distribution function with n close to one. On the other hand, a fracture with just a few tall asperities (i.e. only a few with small shortness) would be characterised by a large n value. Gangi noted that the first case would be representative of a well-polished surface, while the latter would be representative of a new fracture with just a few large intact asperities.

Gangi (1978) derived the following equation for the spacing between the fracture faces w subject to an external stress $P = F/(DL)$ (Figure 3a),

$$w/w_0 = 1 - \left(\frac{P}{K_{asp}}\right)^m \tag{8a}$$

Or in terms of reduction in the fracture spacing

$$x/w_0 = \left(\frac{P}{K_{asp}}\right)^m \tag{8b}$$

where K_{asp} is the effective modulus of the asperities ($K_{asp} = E_{asp}A_r/A$, where A_r/A is the fractional area contact of the crack faces) and is typically of the order of one-tenth to one-hundredth of the asperity material bulk modulus. The exponent m (m=1/n, $0 < m < 1$) is a constant that characterises the distribution function of the asperity heights, with low/high values representing relatively rougher/smoother fracture surfaces.

Thus the permeability variation for the fracture is given by

$$k_f = k_{f0}[1 - \left(\frac{P}{K_{asp}}\right)^m]^3 \tag{9}$$

where k_{f0} is the fracture permeability at zero effective stress.

In the derivation of Equation (8), Gangi assumed, for mathematical convenience and simplicity, that the rods have the same spring constant, which provides the resistance to deformation. The spring constant for a rod is given by

$$k_i = Ea_i / l_i \tag{10}$$

where E and a_i are the Young's modulus and cross-sectional area of the rods, respectively. If the rods are made of the same material and they all have the same Young's modulus, E, then this requires that the cross-sectional area proportional to the length of the rods. It was further implicitly assumed that the spring constant of the rods would remain unchanged during rod deformation. The implication of this latter assumption will be discussed later.

Walsh (1981) considered fractures with an exponential size distribution of asperities and found the permeability to vary as

$$k_f = k_{ref}[1 - \sqrt{2}h/a_{ref} ln\left(\frac{P}{P_{ref}}\right)]^3 \quad (11)$$

where k_{ref} is the permeability at reference stress P_{ref}, h is the root-mean-square height distribution of asperities, and a_{ref} is the half width of the fracture aperture at the reference stress P_{ref}. An advantage of this model over Gangi's model (Equation (9)) is that it can be applied, in a straight forward way, to fit the experimental data though linear regression between $k^{1/3}$ and lnP_e. However, unlike Gangi's model, the equation does not contain any elastic properties of the asperities. Other fracture permeability models have also been proposed, of which an excellent review is given by Rutqvist and Stephansson (2003).

Previous studies of shale permeabilities have shown that both exponential and power law equations appear to yield good fit to the experimental data (e.g. Katsube et al., 1991; Vasseur et al., 1995; Dewhurst et al., 1999; Dong et al., 2015). Bustin et al. (2008) reported shale permeabilities and their variation with effective stress for several shales (Figure 4). We found that the digitized permeability data from the original publication, which span over 3 orders of magnitude, can be fitted well using an exponential function of the effective stress P_e with a constant compressibility coefficient c_{exp},

$$k_{exp} = k_0 e^{-c_{exp} P_e} \quad (12)$$

The compressibility coefficient ranges from 5.07x10^{-4} to 1.33x10^{-3} psi^{-1} (7.35x10^{-2} to 0.193 MPa^{-1}) for the five shales.

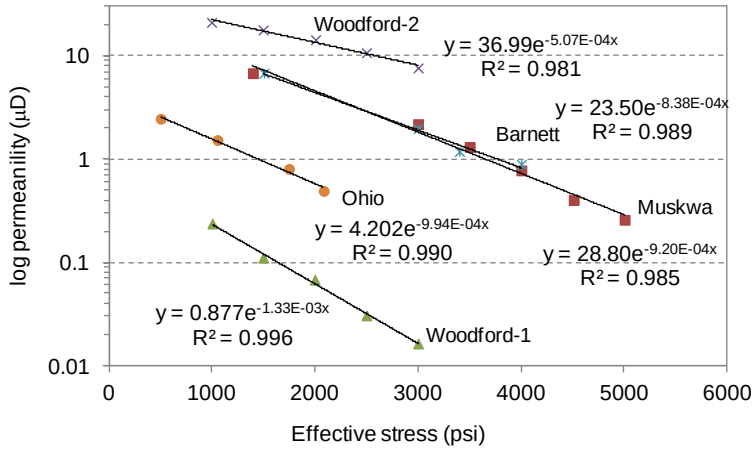

Figure 4 Experimental permeability data of different shales displaying exponential relationship with effective stress (modified from Bustin et al., 2008)

At a first glance there exists a mismatch between the above power law/logarithmic theoretical models and the experimental permeability data that exhibit exponential or near-exponential effective stress dependency. In this study, an in-depth analysis has been carried out to ascertain whether these models could be applied to describe the experimental permeability, which is of practical interest. In particular, the power law models by Gangi are analysed to evaluate their predictability of the near-exponential permeability behaviour. It will be shown that Gangi's power equations for both intact and fractured rocks can be approximated by

exponential equations over certain ranges of effective stress. The two models are then applied to the comprehensive permeability data for a number of gas shales recently published by Heller et al. (2014) and the results are presented and discussed.

2. Near-exponential relationship in the theoretical models

In this section Gangi's models for intact and fractured rocks are revisited to reveal the hidden near-exponential relationship between rock permeability and the applied effective stress.

2.1 Intact rock

Equation (6) maybe rearranged as

$$\frac{k_{wr}}{k_{lp}} = [1 - \left(\frac{P_e+P_i}{K'}\right)^{\frac{2}{3}}]^4 \tag{13}$$

where

$$K' = K_{gra}/C_0^{1.5} \tag{14}$$

Note that the external stress P is replaced by the effective stress P_e. Parameter K' may be considered as an apparent bulk modulus of the porous rock which takes into account the grain packing as well as the grain elastic modulus. Packing constant C_0 for a uniform packing arrangement can be computed. It can be shown that (Figure 1a)

$$r_p = R/\cos\theta - R$$

With $\theta = 30^o$ (Figure 1a), $r_p/R = 0.155$. It follows that

$$C_0 = \frac{2c_1R}{r_p} \cong \frac{1}{0.155\cos(30^o)} = 7.46$$

In other words, C_0 is of order of 7.5, rather than 2 as reported by Gangi (1978). Thus, one has

$$K' \cong K_{gra}/20 \tag{14a}$$

Figure 5a presents a semi-log plot of $\frac{k_{wr}}{k_{lp}}$ as a function of the normalised effective stress $\frac{P_e+P_i}{K'}$. It can be seen that Gangi's model predicts a steady reduction in permeability with an increasing (applied) effective stress. Examination of the plot reveals that the permeability reduction over a certain range of the normalized effective stress is very close to exponential (following a straight line).

The fitted exponential equation has the form (Figure 5b)

$$\frac{k_{wr}}{k_{lp}} \cong 0.797\mathrm{e}^{-7.238\frac{P_e+P_i}{K'}} \tag{15}$$

The difference between the exponential Equation (15) and Gangi's Equation (13) is within 5% over the normailised effective stress range (Figure 5c)

$$0.03 \leq \frac{P_e+P_i}{K'} \leq 0.44 \tag{16}$$

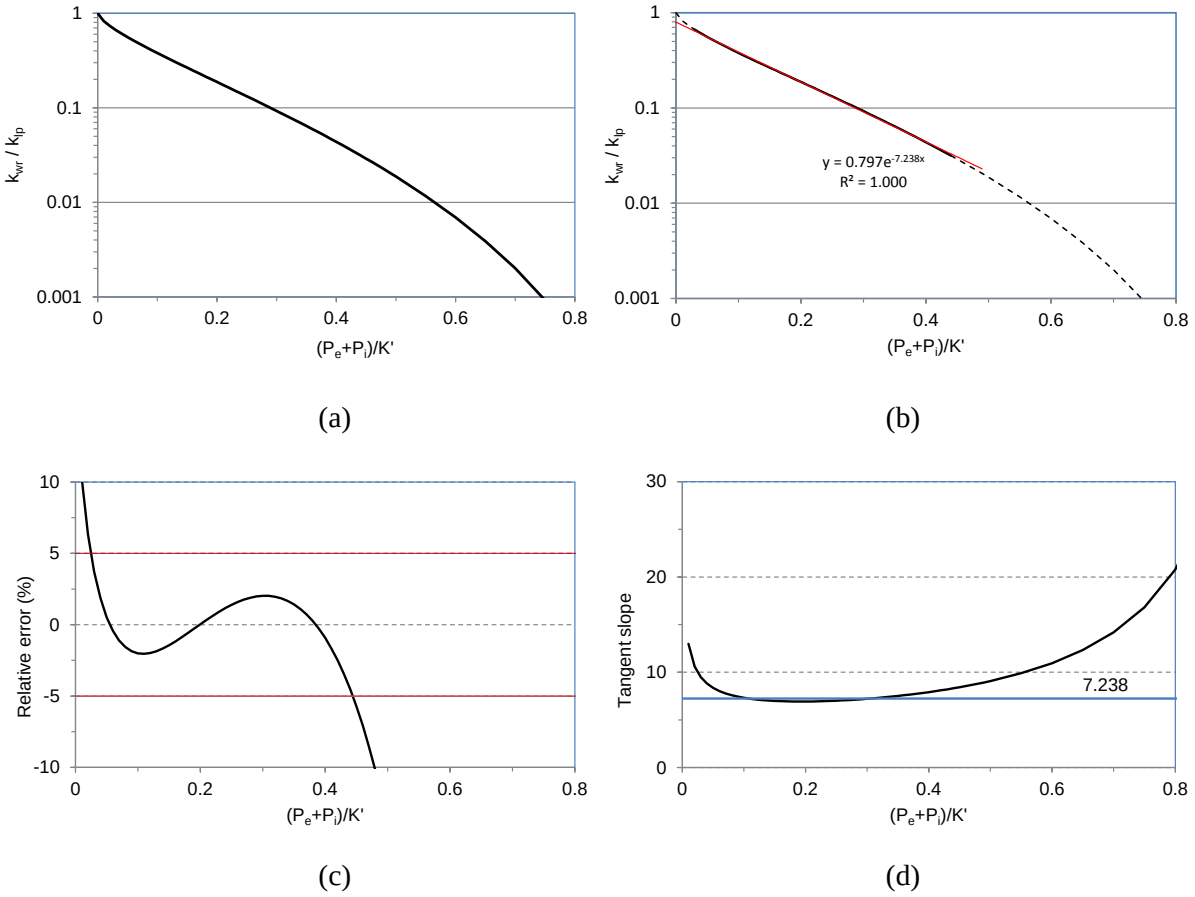

Figure 5 a) Semi-log plot of intact rock permeability ratio with respect to the normalised total effective stress from Gangi's model; b) near-exponential relationship within a certain effective stress range identified in this study; c) Relative error between Equations (15) and (13); d) The slope of tangent to the semi-log permeability curve shown in a).

The slope of the tangent to the semi-log permeability-effective stress curve can be found from Equation (13) as

$$tangent\ slope = \frac{dln\frac{k_{wr}}{k_{lp}}}{d(\frac{P_e+P_i}{K'})} = -\frac{8}{3(\frac{P_e+P_i}{K'})^{1/3}[1-(\frac{P_e+P_i}{K'})^{2/3}]} \tag{17}$$

As shown in Figure 5d, the tangent slope curve remains largely flat within the normalised effective stress range [0.03, 0.44], Figure 5d. This suggests that the two terms in the denominator of the right-hand-side of Equation (17) compensate each other to a large extent over this stress range. This appears to be an interesting property of the power-law functions, as we shall come across later.

Given $K_{gra} \cong 20K'$ (assuming C_0 = 7.5), the normalized total effective stress range [0.03, 0.044], with respect to K', is equivalent to [0.0015, 0.022] with respect to K_{gra}. Therefore the effective stress P_e of interest here is well within the limit (< $0.03K_{gra}$) for which Gangi's model is considered to be valid. The near-exponential permeability reduction over this stress range is over one order of magnitude (a factor of 20).

Denoting

$$k_{wri} = 0.797 k_{lp} \mathrm{e}^{-7.238\frac{P_i}{K'}} \tag{18}$$

Equation (15) becomes

$$k_{wr} \cong k_{wri} \mathrm{e}^{-7.238\frac{P_e}{K'}} \qquad 0.03 - \frac{P_i}{K'} \leq \frac{P_e}{K'} \leq 0.44 - \frac{P_i}{K'} \tag{19}$$

2.2 Fractured rocks

Equation (9) may be rewritten as

$$\frac{k_f}{k_{f0}} = [1 - \left(\frac{P_e}{K_{asp}}\right)^m]^3 \tag{20}$$

where the external stress P is replaced by the effective stress P_e. The permeability behaviour of fractured rocks under loading is dependent on the asperity-length distribution in the fractures, which is characterised by parameter m (= 1/n). Semi-log plots of $\frac{k_f}{k_{f0}}$ as a function of the normailised effective stress $\frac{P_e}{K_{asp}}$ for different values of m are presented in Figure 6.

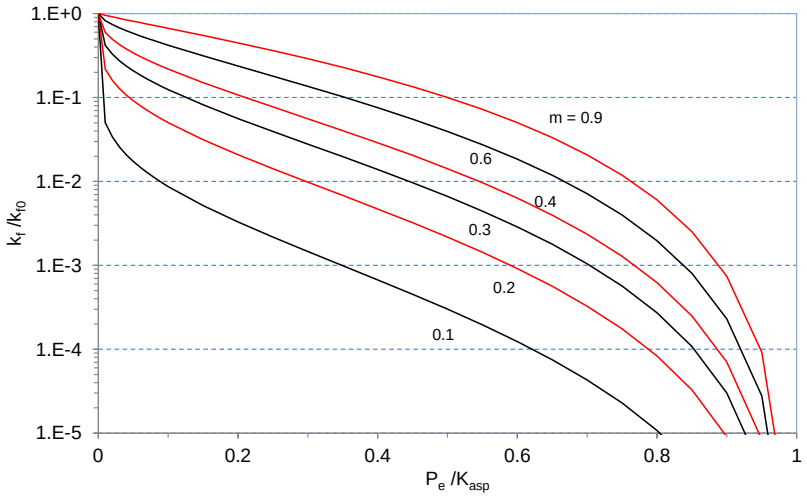

Figure 6 Semi-log plot of fractured rock permeability ratio with respect to the normalised effective stress from Gangi's model for m ranging from 0.1 to 0.9.

It can be seen that the overall fracture permeability behavior is strongly influenced by the fracture surface characteristics. For small m (< 0.4), an initial sharp drop in the permeability of up to over one order of magnitude is observed at small P_e; the permeabilities then follow a broadly similar trend of steady reduction with further increasing in the effective stress. The initial sharp reduction in permeability for small m (n > 5) can be attributed to their asperity-length distributions where there are very few tall rods (small shortness) and an overwhelming majority of the rods have a height less than $0.3w_0$ (shortness > $0.7w_0$) (Figure 3b).

Examination of each individual permeability curve with representative value of m (0.1, 0.2, …, 0.9) across its range reveals that a stage of near-exponential permeability reduction can be identified for all the curves, albeit generally over different ranges of the normalised effective stress (Figure 7).

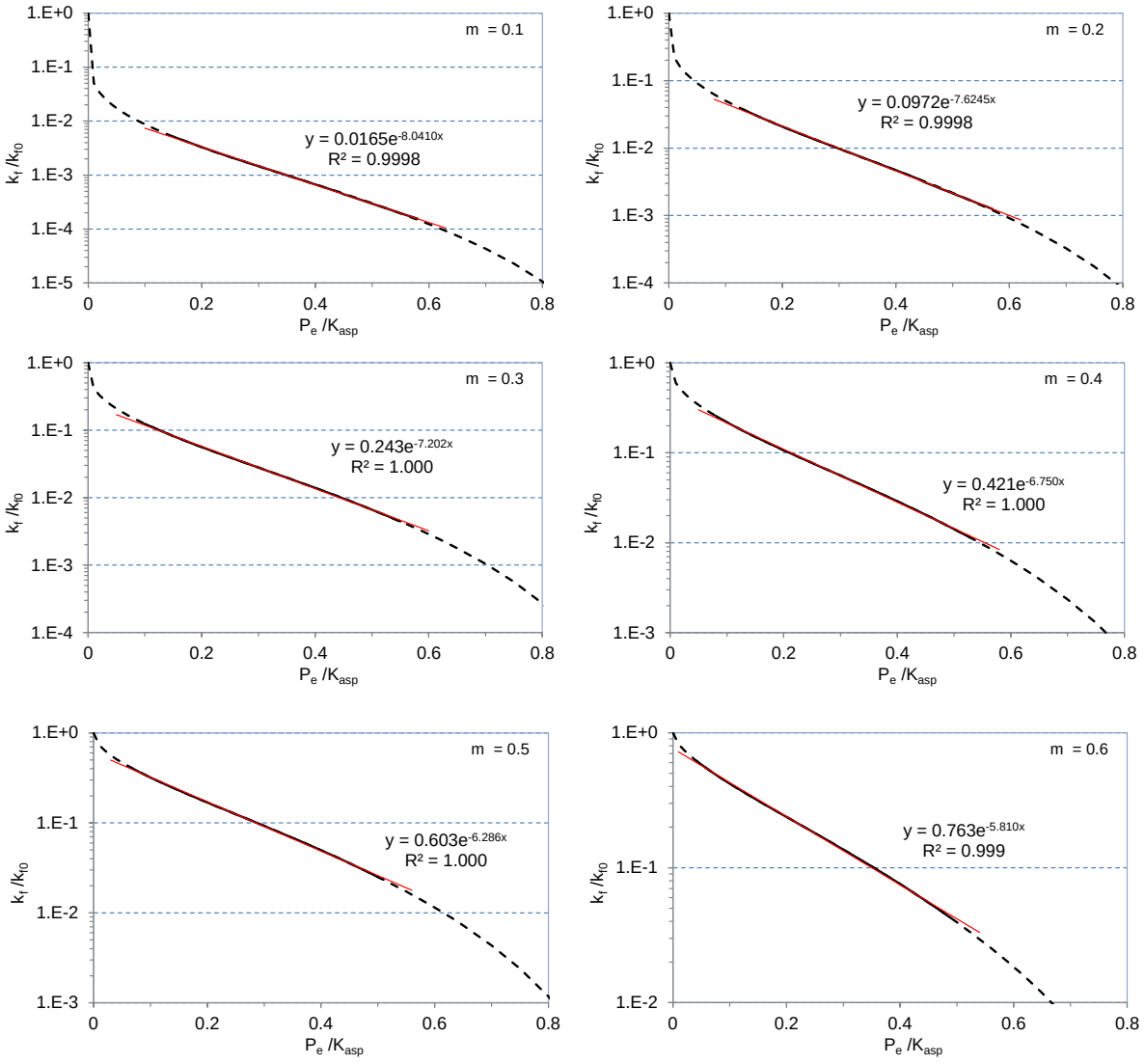

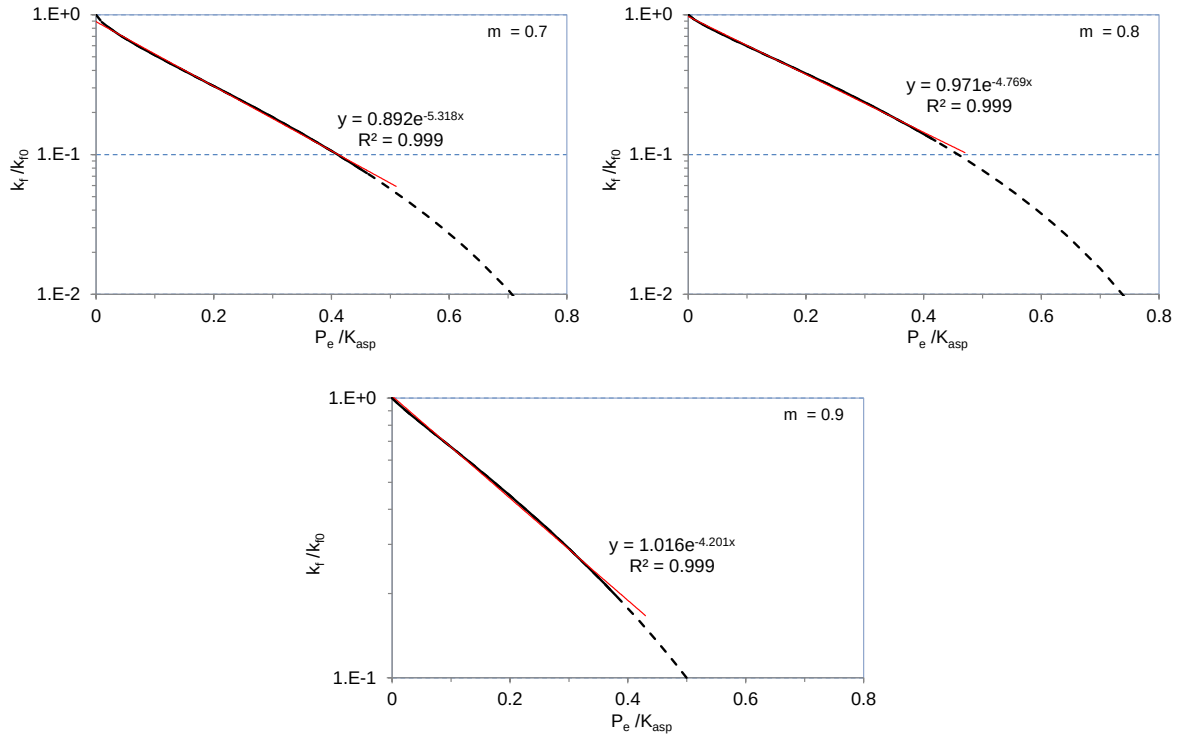

Figure 7 Near-exponential relationships between fractured rock permeability and normalised effective stress identified for different values of *m* across its range (0, 1) in this study.

The fitted exponential equations for all the curves have a similar form as Equation (15)

$$\frac{k_f}{k_{f0}} \cong A_m \mathrm{e}^{-B_m \frac{P_e}{K_{asp}}} \tag{21}$$

where A_m and B_m are constant coefficients corresponding to a given m. The difference between the exponential Equation (21) and Gangi's model Equation (20) is within 5% over the normalised effective stress range

$$a_m \leq \frac{P_e}{K_{asp}} \leq b_m \tag{22}$$

The coefficients, together with the corresponding stress ranges, are presented in Table 1. It is noted that the coefficient A_m increases by almost two orders of magnitude, from 0.0165 to 1.016 as m varies from 0.1 to 0.9, whereas the corresponding coefficient B_m lowering by approximately 50%, from 8.0 to 4.2. It is further noted that coefficient B_m appears to reduce lineally with increasing m (Figure 8)

$$B_m = 8.609 - 4.773m \tag{23}$$

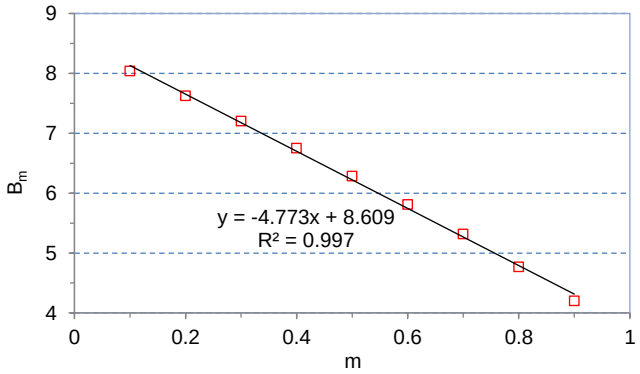

Figure 8 A linear correlation between coefficient B_m and parameter m.

While the size of the normalised effective stress range remains largely unchanged at ~ 0.4, it tends to shift to the left along the effective stress axis, as m is increased. For example, the normalised effective stress range is [0.15, 0.58] for m = 0.1, compared to [0.0, 0.38] for m = 0.9. The corresponding near-exponential permeability reduction ranges from less than a factor of 5 for m = 0.9 to just over two orders of magnitude for m = 0.1.

Table 1 Exponential function coefficients and associated normalised effective stress range for Gangi's fracture permeability model

m	A_m	B_m	a_m	b_m
0.1	0.0165	8.041	0.15	0.58
0.2	0.0972	7.625	0.13	0.57
0.3	0.243	7.202	0.1	0.55
0.4	0.421	6.750	0.08	0.53
0.5	0.603	6.286	0.06	0.51
0.6	0.763	5.810	0.04	0.49
0.7	0.892	5.318	0.01	0.46
0.8	0.971	4.769	0.0	0.42
0.9	1.016	4.201	0.0	0.38

The slope of the tangent to the semi-log permeability-effective stress curves in Figure 6 can be found from Equation (20)

$$tangent\ slope = \frac{dln\frac{k_f}{k_{f0}}}{d(\frac{Pe}{K_{asp}})} = -\frac{3m}{(\frac{Pe}{K_{asp}})^{1-m}[1-(\frac{Pe}{K_{asp}})^m]} \tag{24}$$

The similarity between Equation (24) and Equation (17) is observed. Indeed, the two equations have the same functional expression when m = 2/3. Therefore, Equation (17) may

be viewed as a special case for Equation (24). It would thus appear that the near-exponential behavior is something inherent in the power-law function permeability models.

Equation (21) may be rewritten as

$$k_f \cong k_{fi} \mathrm{e}^{-B_m \frac{P_e}{K_{asp}}}, \qquad a_m \leq \frac{P_e}{K_{asp}} \leq b_m \tag{25}$$

where $k_{fi} = A_m k_{f0}$.

2.3 Remarks on the assumptions and validity of the permeability models

The above analysis has shown that both Gangi's permeability equations for intact and fractured rocks, irrespective of their contrasting physical models, predict a near-exponential relationship between permeability and effective stress over certain effective stress ranges. This is an important finding as this permeability behaviour has been widely reported for different porous rocks, intact or fractured alike.

It has been further elucidated that this near-exponential dependency in Gangi's permeability models arises from their essentially power-law function formulation. Incidentally, both the (elastic) deformation of grain spheres given by Hertz's theory (Equation (2)) and reduction in the fracture spacing derived by Gangi (Equation (8b)) are power-law functions of the (normalised) effective stress.

It has been shown that Gangi's permeability model for intact rocks can be closely approximated (within 5%) by an exponential equation

$$k_{wr} \cong k_{wri} \mathrm{e}^{-7.238 \frac{P_e}{K'}} \qquad 0.03 - \frac{P_i}{K'} \leq \frac{P_e}{K'} \leq 0.44 - \frac{P_i}{K'} \tag{19}$$

The transformed exponential equation yields a semi-empirical pore compressibility of

$$c_p = \frac{7.238}{K'} \tag{26}$$

The apparent bulk modulus of the porous rock K' maybe estimated by comparing Equation (26) with the experimentally arrived compressibility (Equation 12)

$$K' = \frac{7.238}{c_{exp}} \tag{27}$$

The predicted near-exponential permeability reduction is over one order of magnitude (a factor of 20) as the rock grains deform elastically. The permeability model becomes invalid when rock grains continue to deform beyond their elastic limits during loading. As the elastic and strength properties vary for different rocks, it maybe expected that the effective stress range over which Gangi's model is valid would vary accordingly.

It has also been shown that Gangi's permeability model for fractured rocks can be closely approximated (within 5%) by the following exponential equations

$$k_f \cong k_{fi}\mathrm{e}^{-B_m\frac{P_e}{K_{asp}}}, \qquad a_m \leq \frac{P_e}{K_{asp}} \leq b_m \tag{25}$$

The transformed exponential equation yields a semi-empirical fracture compressibility of

$$c_f = \frac{B_m}{K_{asp}} \tag{28}$$

Note that c_f is influenced by the smoothness of the fracture surfaces as well as the effective modulus of the asperities. The effective modulus of the asperities K_{asp} maybe estimated by comparing Equation (28) with the experimentally arrived compressibility (Equation 12)

$$K_{asp} = \frac{B_m}{c_{exp}} \tag{29}$$

The predicted near-exponential permeability reduction ranges from less than a factor of 5 (m = 0.9) to just over two orders of magnitude (m = 0.1).

Note that in this study the fracture compressibility is defined with respect to the effective stress as

$$c_f = -\frac{1}{\phi_f}\frac{\partial \phi_f}{\partial P_e} \tag{30}$$

where ϕ_f is the fracture porosity. It has been shown in the literature that Equation (30) maybe integrated to yield an exponential relationship between fracture porosity/fracture permeability and the effective stress. If we assume that the compressibility remains unchanged within the range of effective stress of interest, Equation (30) maybe integrated as

$$\phi_f = \phi_{f0}e^{-c_f(P_e - P_{e0})} \tag{31}$$

where ϕ_{f0} is the porosity at reference effective stress P_{e0}. Substituting porosity with permeability using the cubic relationship between the fracture porosity and the fracture permeability leads to the following exponential relationship between fracture permeability and effective stress

$$k = k_0 e^{-3c_f(P_e - P_{e0})} \tag{32}$$

The analysis in this study has shown that the assumption of constant fracture compressibility maybe justified over certain ranges of effective stress according to Gangi's model.

In Gangi's fractured rock model the springs of the rods representing the asperities are assumed to remain unchanged during deformation. This is clearly an approximation as in reality the spring of rods, defined as the product of the Young's modulus of asperities and the ratio of cross-section area of a rod over its height (Equation (10)), is expected to increase under compressive deformation - a reduction in the height is accompanied by an corresponding increase in its cross-section. Furthermore, the cross-section area of a rod is unlikely to be uniform along its height, with the narrowest section of the rod being deformed

first. Therefore Gangi's model tends to underestimate the rod spring constant, and thus overestimate the permeability reduction, especially when the (normalised) effective stress becomes large (beyond ~0.5). Nevertheless, the assumption of a constant rod spring appears to be adequate for many applications. Kwon et al. (2001) noted that values of K_{asp} inferred from fitting the experimental permeability data using Gangi's model correlate with the effective stresses at which permeabilities were measured, and proposed that systematical variations in $K_{asp}$with P_e are due to inelastic changes in loaded asperity dimensions.

In order to better fit some permeability data of coal seams at depths, McKee et al. (1988) proposed a fracture compressibility which declines exponentially with increasing effective stress

$$c_f = c_{f0} e^{-\alpha(P_e - P_{e0})} \tag{33}$$

where c_{p0} is the compressibility at initial effective stress P_{e0} and α is a constant. Equation (32) then becomes

$$k = k_0 e^{-3\bar{c}_f(P_e - P_{e0})} \tag{34}$$

where $\bar{c}_f$is the mean compressibility over the effective stress range [P_{e0}, P_e]

$$\bar{c}_f = \frac{c_{f0}}{\alpha(P_e - P_{e0})}(1 - e^{-\alpha(P_e - P_{e0})}) \tag{35}$$

A similar approach may be applied in the transformed Equation (19) to account for the effects of an increasing rod spring (thus K_{asp}) on the permeability response.

3. Application to gas shales

Four types of porous media are present in productive gas-shale systems: the nonorganic matrix, the organic matrix, natural fractures, and hydraulic fractures (Wang et al., 2009). Gas permeability in organic matter, where adsorbed as well as free gases can be stored, is significantly higher than that in the nonorganic matrix, due to its high porosity. It has been reported that permeability values measured using core plugs can be orders of magnitude higher that those measured using crushed samples, suggesting that the permeability of core plugs is predominantly due to the organic and microfracture pore network present (e.g. Wang et al., 2009). Figure 9 presents a schematic diagram showing high-permeability elements in gas shale.

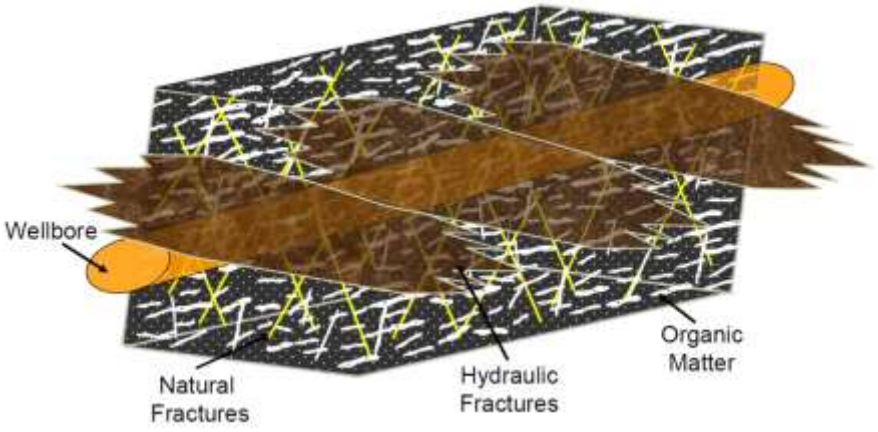

Figure 9 Schenatic diagram showing high-permeability elements in gas shale: organic matter, natural fractures, and hydraulic fractures (after Wang et al., 2009).

Gangi's model for fractured rocks (Equation (9)) has been used by Kwon et al. (2001) to fit the permeability of Wilcox shale. In the current work, Gangi's transformed permeability models for intact (Equation (19)) as well as for fractured (Equation (25)) rocks have been applied to a set of comprehensive helium gas permeability data for core samples of six different gas shales recently reported by Heller et al. (2014). The purposes of the study were two-folds: 1) to demonstrate the application of the transformed models; 2) to estimate the relevant elastic property of the rock (K') and asperities (K_{asp}) for the tested samples. It needs to be pointed that the rock/fracture properties thus obtained reflects the underlying physical model used. In other words, the measured reductions in the shale plug permeability are assumed to be predominantly due to either the deformation of sphere grains in packing or the narrowing of the fracture apertures. In reality the measured permeability behaviour of the gas shales is likely to be a combination of these two mechanisms.

A notable feature of Heller's permeability data is that the effective stress law for the core samples has been established experimentally. This was achieved by varying the confining pressure (P_c) and the flowing gas pressure (P_p) independently during a test. The pore pressure varied from 1,000 to 4,000 psi (6.9 to 27.6 MPa) in steps and the corresponding effective confining pressure ranged from ~1,000 psi to ~5,000 psi (~6.9 to 34.5 MPa). The permeability data used in this study have been digitized from the original publication and are given in Table A-1 in the Appendix.

The effective stress is expressed as

$$P_e = P_c - \chi P_p$$

where is χ the effective stress coefficient. It may be determined by (Kwon et al., 2001)

$$\chi = -\frac{\partial log k/\partial P_c}{\partial log k/\partial P_P}$$

The effective stress coefficients determined for the six core samples vary from 0.15 to 0.85, Table 2 (column 2).

Table 2 Results of fitting the experimental data by Heller et al. (2014) using an exponential equation

	χ	Fitted coefficients	
		k_0, μD	c_{exp} 10^{-4} psi^{-1} (10^{-2} MPa^{-1})
Barnett 27	0.82	2.25	2.30 (3.34)
Barnett 31	0.68	2.03×10^{-1}	2.27 (3.29)
Eagle Ford 127	0.6	15.1	1.60 (2.32)
Eagle Ford 174	0.4	9.56×10^{-2}	5.68 (8.23)
Marcellus	0.15	8.65×10^{-2}	2.24 (3.25)
Montney	0.85	17.9	2.02 (2.93)

As shown in Figure 10, the permeability data by Heller et al. (2014) can be fitted reasonably well using exponential equations, with $R^2 > 0.97$ for all the six samples. The fitted coefficients (k_0 and c_{exp}) are summarised in Table 2 (columns 3 and 4). The pore/microfracture compressibility c_{exp} ranges from 1.60 to 5.68×10^{-4} psi $^{-1}$ (2.32 to 8.23×10^{-2} MPa^{-1}). It needs to be pointed out that the set of permeability data by Heller et al. (2014) may also be fitted using other equations. Indeed, we found that good match could be achieved using Gash's model Equation (11) (results not shown here).

3.1 Gangi's intact rock model

Using Equation (27), the apparent bulk modulus K' for the six core samples tested by Heller et al. (2014) could be determined (Table 3, column 2). Among the six samples, Eagle Ford 174 has the lowest K' (~ 80 MPa) due to its relatively large compressibility. The apparent bulk modulus for the other five samples lies in the range between ~200 and ~300 MPa. The corresponding effective grain elastic moduli K_{gra} are of the order of several GPa with C_0 = 7.5 (Table 3, column 3). The estimation of the apparent bulk modulus for each sample allows the range of normalised effective stress P_e/K' to be determined (Table 3, column 4). It is noted that the normailsed effective stresses are generally less than 0.2, except for Eagle Ford 174 due to its relatively low K'.

We note that the ranges of normalized effective stress obtained for the six samples, with the exception for Eagle Ford 174, fall within the range [0.03- P_i/K', 0.44- P_i/K'] provided $P_i < 0.24K'$. Although the equivalent pressure P_i is generally unknown, it might be speculated that it is more likely to be of order of ~$0.01K'$ (~MPa) than ~ $0.1K'$ (~ tens of MPa).

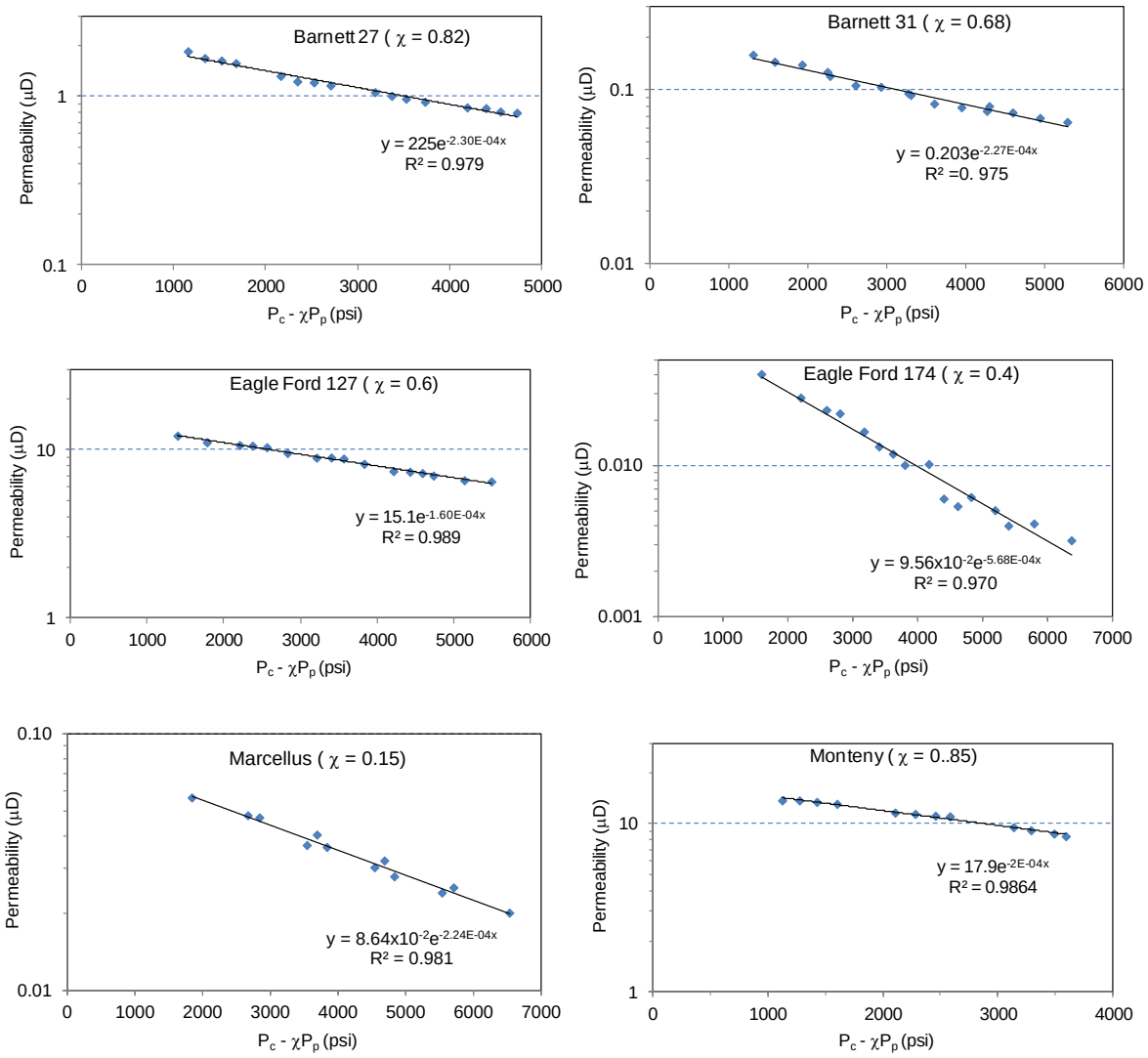

Figure 10 Fitting of the experimental permeability data by Heller et al. (2014) using exponential equations. Note the permeability unit for Barnett 27, Eagle Ford 127 and Montney is μD, as opposed to nD for the other three samples.

Table 3 Results from matching the experimental data by Heller et al. (2014) using the transformed equation of Gangi's model for intact rock

	K', MPa	K_{gra}, GPa (C_0 = 7.5)	P_e/K'
Barnett 27	217	4.5	[0.037, 0.15]
Barnett 31	220	4.5	[0.041, 0.17]
Eagle Ford 127	312	6.4	[0.031, 0.12]
Eagle Ford 174	88.0	1.8	[0.13, 0.50]
Marcellus	222	4.6	[0.057, 0.20]
Montney	247	5.1	[0.031, 0.10]

For demonstration, the predictions by Gangi's original model Equation (5), assuming $P_i = 0.02K'$, for the six samples are compared with the experimental data in Figure 11, where the permeabilities are normalised with respect to k_0. The loose packing permeability k_{lp} in Equation (5) can be found from Equation (18) noting $k_{wri} = k_0$

$$k_{lp} = \frac{e^{7.236\frac{P_i}{K'}}}{0.794} k_0$$

It can be seen that a good overall match to the experimental data is achieved for five sample (Barnett 31, Barnett 27, Eagle Ford 127, Marcellus and Montney), whereas for Eagle Ford 174 a notable deviation away from the exponential trendline at the two highest stress data points is observed.

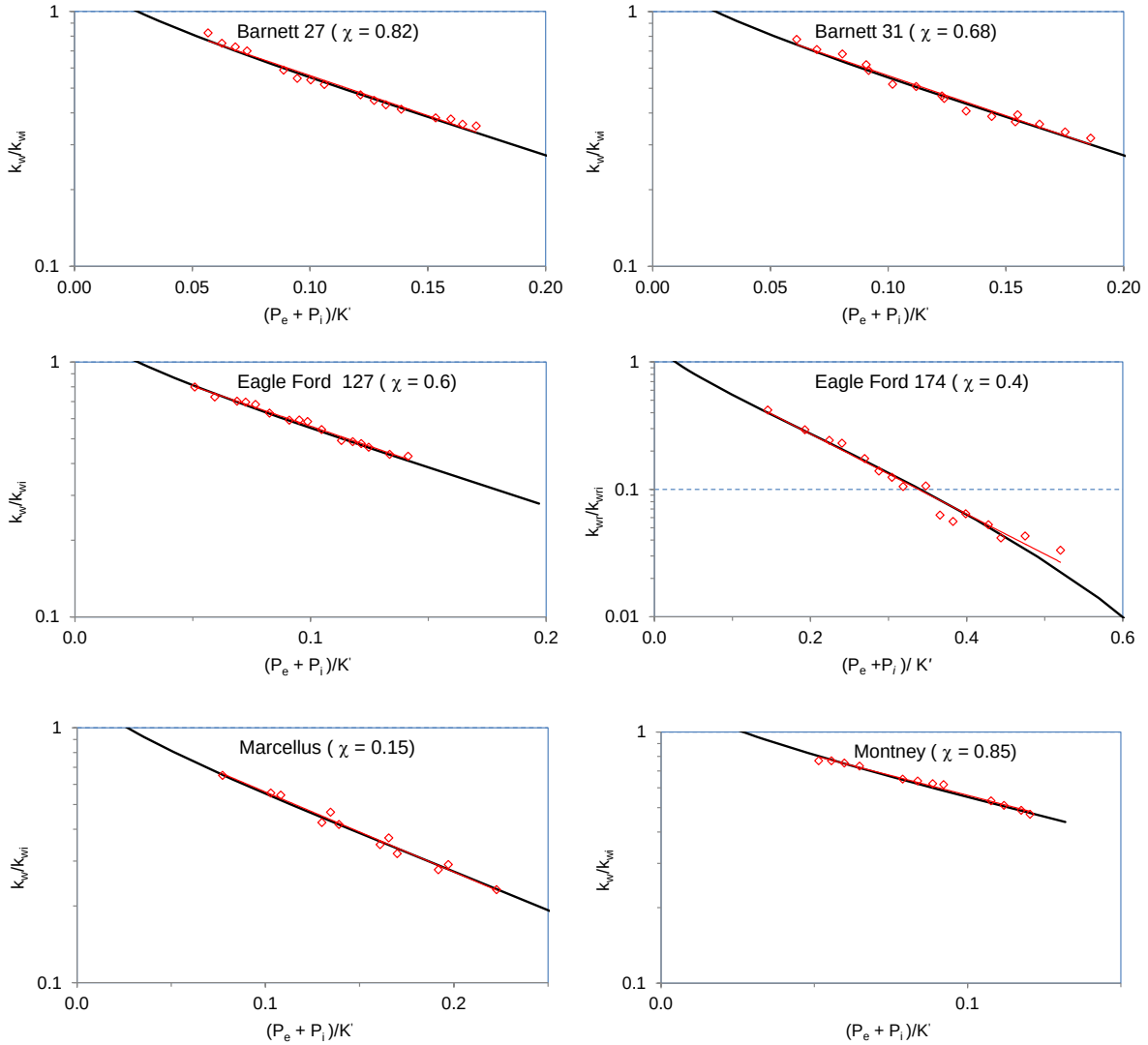

Figure 11 Predictions by Gangi's intact rock model Equation (14) assuming $P_i = 0.02K'$, compared to the experimental data by Heller et al. (2014).

3.2 Gangi's fractured rock model

The values of parameter K_{asp} can be found from Equation (29)

$$K_{asp} = \frac{B_m}{c_{exp}} \tag{29}$$

Recall that B_m ranges from 4.2 (m = 0.9) to 8.0 (m = 0.1) and a linear correlation exists between B_m and m. Clearly the effective modulus of the asperities K_{asp} determined from matching the experimental permeability data is closely related to the smoothness of the fracture surfaces (through coefficient B_m), and is thus unlikely to be unique. It follows that the resulting normalised effective stress P_e/K_{asp} would also vary with m.

Examples of model matching results are presented in Figures 12 (Barnett 31) and 13 (Eagle Ford 174) for m = 0.1, 0.3, 0.5, 0.7, and 0.9. It can be seen from Figure 12 that the permeability data for Barnett 31 can be matched by the model with m = 0.5 to 0.9. Broadly similar outcomes have also been obtained for the other four samples, i.e. Barnett 27, Eagle Ford 127, Marcellus and Montney (results not shown here). On the other hand, a better match is achieved with m residing towards the lower end of its range (m = 0.1 to 0.5) for Eagle Ford 174 (Figure 13). The results for the six gas shales samples in terms of the ranges for parameters m, K_{asp} and k_{f0} (as opposed to k_0 obtained solely from curve fitting the experimental data) and K_{asp} are summarized in Table 4.

Table 4 Results from matching the experimental data by Heller et al. (2014) using the transformed equation of Gangi's permeability model for fractured rock

	m	K_{asp}, MPa	$k_{f0,}$ μD (estimated)	$k_{f0,}$ μD (measured)	$k_{f0}/k_{f0\ measured}$
Barnett 27	0.5 – 0.9	188 - 126	3.7 - 2.2	1.2	2.5
Barnett 31	0.5 – 0.9	191 - 128	0.37 - 0.20	0.1	2.9
Eagle Ford 127	0.7 – 0.9	229 - 181	17.0 - 14.9	9.0	1.7
Eagle Ford 174	0.1 – 0.5	97.7 - 76.3	5.79 - 0.159	1.5×10^{-2}	-
Marcellus	0.5 – 0.9	193 - 129	$14.3 - 8.51 \times 10^{-2}$	3.5×10^{-2}	3.3
Montney	0.7 – 0.9	181 - 143	20.0 - 17.6	11.0	1.7

In the table, larger values of K_{asp} and k_{f0} correspond to lower values of m. The plug permeabilities at zero effective stress for the six samples have been reported by Heller et al. (2014) and are listed in Table 4 (last column) for comparison. There appears to be a typo for Eagle Ford 174 as the reported value of 15 nD (1.5×10^{-2} μD) is lower than those under loading. For the other five samples, the mean of the estimated values are between 1.7 and 3.3 times of the measured values (Table 4 last column).

It is further observed that the effective modulus of the asperities K_{asp} obtained using Gangi' fracture permeability model is broadly the same order of magnitude as the apparent effective bulk modulus K' determined using the model for intact rocks.

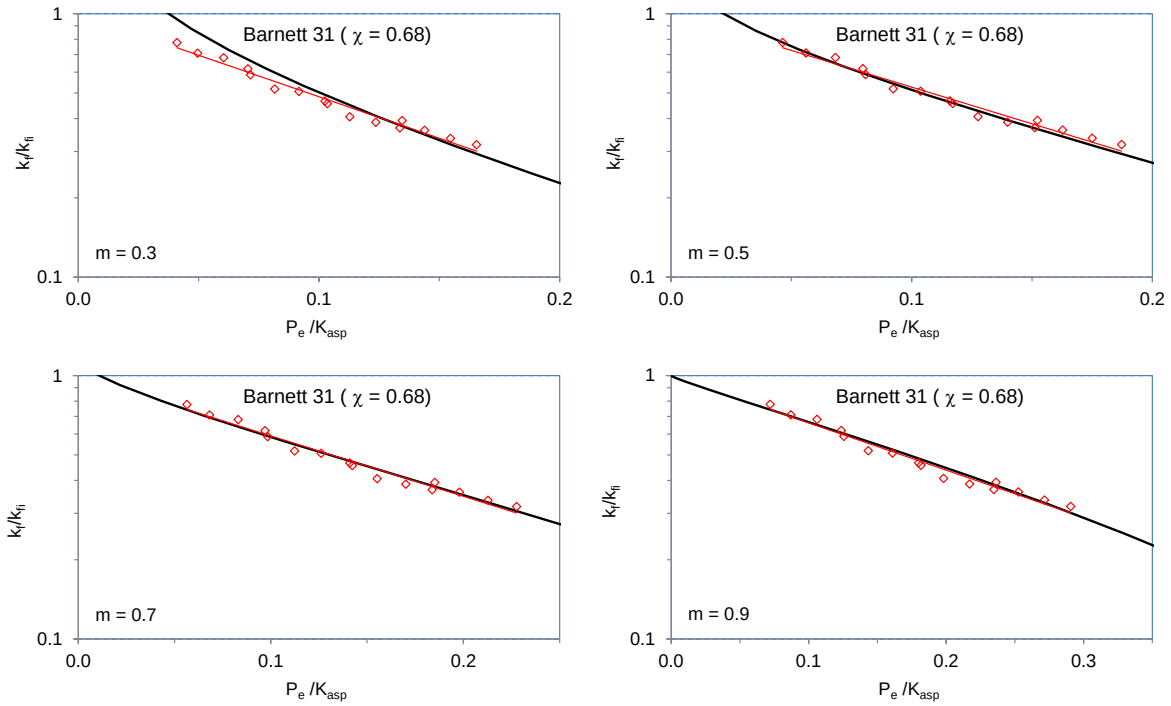

Figure 12 Prediction by Gangi's fracture model Equation (28) for Barnet 31 for a selection of values of *m*, compared to the experimental data. Note K_{asp} is specific to each given *m* in the graphs.

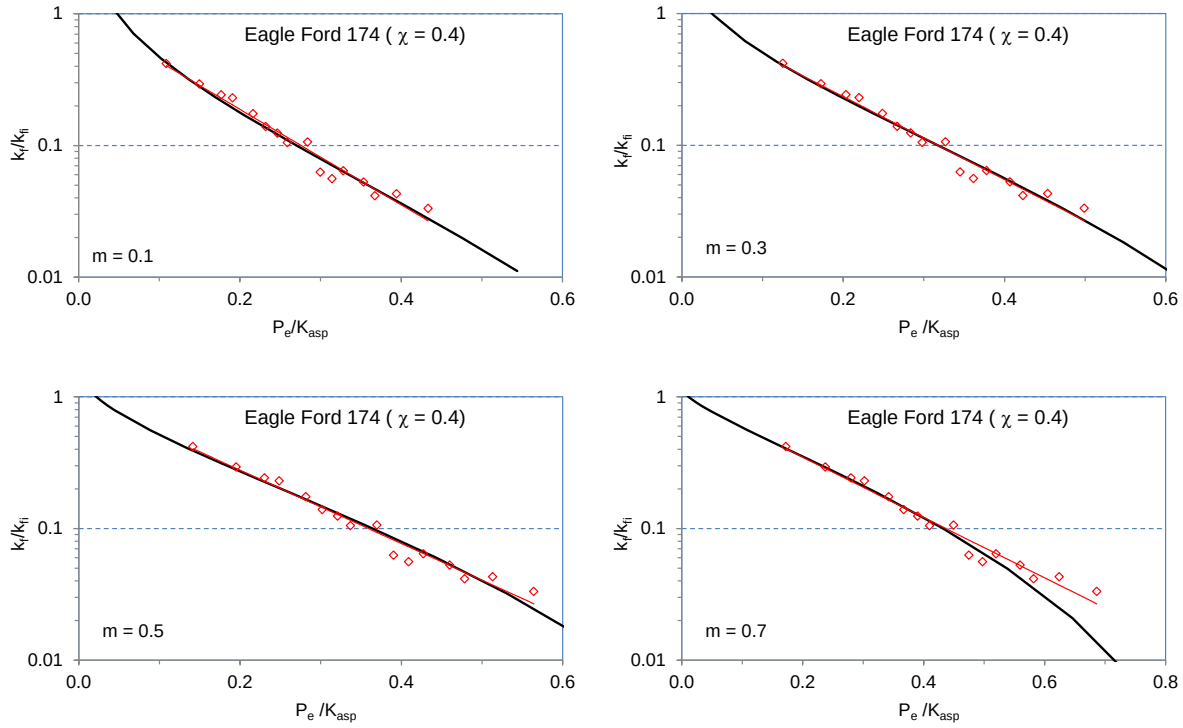

Figure 13 Prediction by Gangi's fracture model Equation (28) for Eagle Ford 174 for a selection of values of *m*, compared to the experimental data. Note K_{asp} is specific to each given *m* in the graphs.

3.3 Discussion

Table 5 summarises the mineralogy of the six samples tested by Heller et al. (2014). Table 6 presents the elastic properties of the main compositional constituents (Quartz, Calcite and clay) and Kerogen reported in the literature. It can be seen that clay and Kerogen have much lower elastic moduli (thus more compressible) than Quartz and Calcite. The estimated effective elastic moduli of the grains K_{gra} using the intact rock model for five of the six shale samples (except Eager Ford 174) fall within the range ~4.5 to ~6.5 GPa (with C_0 = 7.5). The corresponding bulk modulus K ranges from 6.4 to 9.3 GPa ($K_{gra} \approx 0.7K$). We note that the estimated bulk moduli for these five samples are well within the range between that of Kerogen (5 GPa) and clay (12 GPa). Among the five samples, the bulk moduli for Barnett 31, Barnett 27, Macellus and Montney are within a narrower range of 6.4 to 7.3 GPa. On the other hand, the estimated bulk modulus K for Eagle Ford 174 of 1.8 GPa is much lower. Incidentally, a better overall match to Eagle Ford 174 is obtained using the fractured rock model.

Table 5 Mineralogy for the six samples (after Heller et al., 2014)

	Barnett 27	Barnett 31	Eagle Ford 127	Eagle Ford 174	Marcellus	Montney
TOC (%)	3.8	5.3	1.81	4.4	1.17	2.04
Quartz (%)	56.7	51.3	7	16.4	38	42.3
Plagioclase/feldspar (%)	3.8	4	4	1.9	6	11.9
Calcite (%)	7.7	0	80	47.5	1	8.1
Dolomite (%)	1.4	0.4	1	0	1	9.9
Pyrite (%)	1.8	1.7	1	6.7	1	3.5
Apatite (%)	1	0	2	0.6	1	0
Total clay (%)	23.8	37.4	5	22.4	53	24.1

The estimated effective moduli of asperities K_{asp} using the fractured model for the six samples are of orders of ~100 MPa. Recall that K_{asp} is related to the Young's Modulus of the asperities by $K_{asp} = E_{asp}A_r/A$, and is typically of the order of one-tenth to one-hundredth of the asperity material bulk modulus. Therefore the latter is likely to lie in the range between orders of ~1 to ~10 GP. This is comparable with the elastic properties of Kerogen and Clay (Table 6).

Table 6 Elastic properties of main compositional constituents of shale (after Sone, 2012)

	Bulk modulus *K*, GPa	Shear modulus *G*, GPa
Quartz (Mavko et al., 2009)	37	44
Calcite (Mavko et al., 2009)	70.2	29
Clay (Vanorio et al., 2003)	12	6
Kerogen (Bandyopadhyay, 2009)	5	3

In order to explain their experimental permeability data that gave an effective stress coefficient which is less 1, Kwon et al. (2001) proposed a conceptual pore model of shales, where clay forms a connected matrix in which flow paths are located and the effective pore radii are affected to a larger (or an equal) extent to changes in pore pressure than to confining pressure (Figure 14). Heller et al. (2014) found their experimental data support the model by Kwon at al. (2001). This study has provided further and perhaps more compelling evidence in this respect. It has also confirmed the important role played by the organic matrix and connected micronatural fractures in shale gas production.

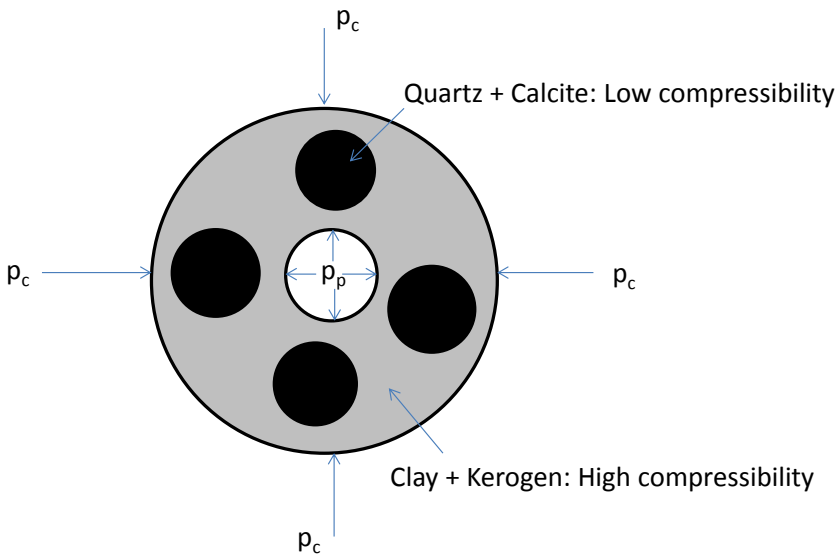

Figure 14 Simplified model pore model for gas shales proposed by Kwon et al. (2001) where clay forms a connected matrix in which flow paths reside (modified from Heller et al., 2014).

5. Conclusions

This study has provided theoretical evidence for the exponential-reduction permeability behavior under loading that has been widely reported for different fractured as well as intact rocks in the literature. The analysis carried out has shown that Gangi's phenomenological permeability models for intact and fractured rocks can be closely approximated by exponential equations over certain ranges of the normalized effective stress. It thus allows for more vigorous theoretical equations to be applied with the easiness of empirical exponential equations.

The near-exponential permeability reduction is over one order of magnitude (a factor of 20) for the intact rock model, and ranges from less than a factor of 5 for $m = 0.9$ to just over two orders of magnitude for $m = 0.1$ for the fractured rock model. Expressions for the compressibilities that are related to the physical property of the rock are obtained.

Application of the transformed equations of the two permeability models indicates that the main gas flow paths for the six core samples reside within the soft constituents (Kerogen + clay) of the rocks.

Acknowledgement

The authors are grateful for the constructive comments of the two anonymous reviewers.

Appendix Experimental permeability data (Heller et al., 2014)

Table A-1 Experimental helium permeability data for six gas shales samples (digitized from Heller et al., 2014)

P_p, psi	Barnett 27 (χ = 0.82)		Barnett 31 (χ = 0.68)		Eagle Ford 127 (χ = 0.6)		Eagle Ford 174 (χ = 0.4)		Marcellus (χ = 0.15)		Montney (χ = 0.85)	
	P_e, psi	k, μD	P_e, psi	k, 10^{-1}μD	P_e, psi	k, μD	P_e, psi	k, 10^{-2}μD	P_e, psi	k, 10^{-2}μD	P_e, psi	k, μD
1,000	1,155	1.85	1,311	1.58	1,397	12.1	1599	4.01	1847	5.63	1,124	13.7
	2,161	1.32	2,288	1.19	2,375	10.5	2601	2.32	2844	4.70	2,105	11.6
	3,187	1.06	3,309	0.925	3,401	8.97	3625	1.19	3841	3.61	3,135	9.51
	4,188	0.86	4,303	0.798	4,427	7.37	4622	0.534	4838	2.77		
2,000	1,338	1.68	1,586	1.44	1,780	11.0	2205	2.80	2673	4.79	1,274	13.7
	2,343	1.23	2,611	1.05	2,830	9.53	3180	1.67	3694	4.03	2,280	11.4
	3,368	1.00	3,607	0.8.26	3,830	8.22	4177	1.02	4691	3.20	3,286	9.12
	4,392	0.85	4,601	0.733	4,733	7.00	5198	0.503	5712	2.51		
3,000	1,519	1.63	1,932	1.38	2,207	10.6	2808	2.20	3547	3.67	1,425	13.4
	2,523	1.21	2,931	1.03	3,210	8.94	3807	1.00	4544	3.01	2,456	11.1
	3,525	0.97	3,952	0.786	4,211	7.44	4827	6.13	5541	2.40	3,487	8.71
	4,549	0.81	4,946	0.684	5,136	6.57	5798	0.410	6538	2.00		
4,000	1,676	1.57	2,255	1.26	2,561	10.3	3412	1.33			1,601	13.1
	2,704	1.16	3,278	0.947	3,562	8.83	4409	0.600			2,582	11.0
	3,730	0.93	4,273	0.749	4,588	7.24	5404	0.397			3,589	8.41
	4,729	0.80	5,291	0.646	5,488	6.46	6374	0.317				

References

Bandyopadhyay, K., 2009, Seismic anisotropy: geological causes and its implications to reservoir geophysics, Ph.D. thesis, Stanford University.

Bustin R.M., Bustin A.M.M., Cui X., Ross D.J.K, Pathi, V.S.M, 2008. Impact of shale properties on pore structure and storage characteristics. In: SPE shale gas production conference. Fort Worth, Texas, USA; 16–18 November 2008.

Chen D., Pan Z., Ye Z., 2015. Dependence of gas shale fracture permeability on effective stress and reservoir pressure: Model match and insights, Fuel **139**:383–392.

Dewhurst D.N., Aplin A.C., Sarda J.-P., 1999. Influence of clay fraction on pore-scale properties and hydraulic conductivity of experimentally compacted mudstones, J. Geophys. Res. **104**:29,261-29,274.

Dobrynin V.M., 1962. Effect of overburden pressure on some properties of sandstones. Soc. Pet. Eragrg. J. **2**:360.

Dong J.J., Hsu J.Y., Wu W.J., Shimamoto T., Hung J.H., Yeh E.C., et al., 2010. Stress dependence of the permeability and porosity of sandstone and shale from TCDP Hole-A. Int J Rock Mech Min Sci **47**:1141–57.

Fatt I. and Davis D. H., 1952. Reduction in permeability with overburden pressure. Trans. Am. Inst. Min. metall. Petrol. Engns **195**:329.

Gangi A.F., 1978. Variation of whole and fractured porous rock permeability with confining pressure. Int J Rock Mech Mining Sci Geomech Abstr **15**:249–257

Gray D. H., Fatt I., Bergamini G., 1963. The effect of stress on permeability of sandstone cores. Son. Pet. Engrg. J. **3**:95.

Heller R., Vermylen J., Zoback M., 2014. Experimental investigation of matrix permeability of gas shales, AAPG Bulletin **98** (5):975–995.

Jones F.O., Jr., 1973. A laboratory study of the effects of confining pressure on fracture flow and storage capacity in carbonate rocks. Soc. Pet. Enono A.I.M.E. 48th Annual Fall Meeting, LasVegas, Nevada. paper No. 4569; also published J. Petrol. Technol. **21** (1975).

Jones F.O. and Ovens W.W., 1980. A laboratory study of low permeability gas sands. J Petrol Eng **32**:1631–1640.

Katsube T.J., Mudford B.S., Best M.E., 1991. Petrophysical characteristics of shales from the Scotian Shelf, Geophysics **56**:1681-1689.

Knutson C. F. and Bohor B. F., 1963. Reservoir rock behavior under moderate confining pressure. Fifth Syrup. on Rock Mechanics (Edited by C. Fairhurst) p. 627. Pergamon Press, New York.

Kranz R. L., Frankel A.D., Engelder T., Scholz C.H., 1979. The permeability of whole and jointed barre granite. Int J Rock Mech Mining Sci Geomech Abstr **16**:225–234.

Kwon O., Kronenberg A.K., Gangi A.F., Johnson B., 2001. Permeability of Wilcox shale and its effective pressure law, Journal of Geophysical Research **106** (B9):19,339-19,353, September 10, 2001.

Louis C., Dessenne J.-L., Feuga B., 1977. Interaction between water flow phenomena and the mechanical behavior of soil or rock masses. In: Gudehus G (ed) Finite elements in geomechanics. Wiley, New York, pp 479–511.

Mavko, G., Mukerji, T., and Dvorkin, J., 2009, The Rock Physics Handbook Second Edition, Cambridge University Press.

McKee C.R., Bumb A.C., Koenig R.A., 1988. Stress-dependent permeability and porosity of coal and other geologic formations. SPE Form Eval. **3**:81–91.

Nelson R., 1975. Fracture permeability in porous reservoirs: experimental and field approach. Ph.D. Dissertation, Department of Geology, Texas A & M University, College Station, TX 77843.

Rutqvist J. and Stephansson O., 2003. The role of hydromechanical coupling in fractured rock engineering, Hydrogeology Journal **11**:7–40.

Sone H., 2012. Mechanical properties of shale gas reservoir rocks and its relation to the in-situ stress variation observed in shale gas reservoirs, Ph.D. thesis, Stanford University.

Tiller F. M., 1953. Chem. Engng Prog. **49**:467.

Vanorio, T., Prasad, M., and Nur, A., 2003, Elastic properties of dry clay mineral aggregates, suspensions and sandstones: Geophysical Journal International, 155, 319-326.

Vasseur G., Djeran-Maigre I., Grunberger D., Rousset G., Tessier D., Velde B., 1995. Evolution of structural and physical parameters of clays during experimental compaction Mar. Pet. Geol. **12**:941-954.

Walsh J.B., 1981. Effects of pore pressure and confining pressure on fracture permeability. Int J Rock Mech Mining Sci Geomech Abstr **18**:429–435.

Wang F.P., Reed R.M., John A., Katherine G., 2009. Pore networks and fluid flow in gas shales. In: SPE annual technical conference and exhibition. New Orleans,Louisiana, USA; 4–7 October 2009.

Witherspoon P.A. and Gale J.E., 1977. Mechanical and hydraulic properties of rocks related to induced seismicity. Engmt Geol. **11**: 23-55 (1977)